photonics

MDPI

Communication

Advantages of Using Hard X-ray Photons for Ultrafast Diffraction Measurements

Vladimir Lipp [1,2,*], Ichiro Inoue [3] and Beata Ziaja [1,2,*]

[1] Institute of Nuclear Physics, Polish Academy of Sciences, Radzikowskiego 152, 31-342 Kraków, Poland
[2] Center for Free-Electron Laser Science CFEL , Deutsches Elektronen-Synchrotron DESY, Notkestr. 85, 22607 Hamburg, Germany
[3] RIKEN SPring-8 Center, 1-1-1 Kouto, Sayo 679-5148, Hyogo, Japan; inoue@spring8.or.jp
* Correspondence: vladimir.lipp@desy.de (V.L.); ziaja@mail.desy.de (B.Z)

Abstract: We present a comparative theoretical study of silicon crystals irradiated with X-ray free-electron laser pulses, using hard X-ray photons of various energies. Simulations are performed with our in-house hybrid code XTANT based on Monte Carlo, Tight Binding and Molecular Dynamics simulation techniques. By comparing the strength of the coherently scattered signal and the corresponding electronic radiation damage for three X-ray photon energies available at the SACLA free-electron laser facility, we conclude that it would be beneficial to use higher photon energies for "diffraction-before-destruction" experiments.

Keywords: X-ray diffraction; X-ray; computer simulation; diffraction before destruction

1. Introduction

X-ray free-electron lasers (XFELs) provide ultrashort X-ray pulses with unique characteristics, such as high spatial and temporal coherence, unprecedented brilliance, and MHz repetition rates [1–3]. Thanks to these characteristics, they enable applications that were not feasible with the synchrotron or high-harmonic generation sources, such as studies of ultrafast structural transformations with pump-and-probe experiments and "diffraction-before-destruction" applications [4–7]. The latter can provide opportunities for the structure determination of radiation-sensitive samples, but they also introduce many challenges [8], such as a potential target disordering during diffraction, which can deteriorate the quality of structure determination. In an earlier work, we showed that the X-ray-induced electron cascading can cause a delay in the structural changes at high photon energies [9,10], which could improve the reliability of "diffraction-before-destruction" applications for sufficiently short pulse durations.

Although the "diffraction-before-destruction" concept has been successfully applied to many protein crystals and has enabled the identification of their atomic structure [11,12], it is not clear whether one can realize advanced structure determination with this concept, going beyond the determination of atomic positions. Namely, the visualization of electron density distribution in chemical bonds and molecular orbitals still remains a challenge with ultrafast X-ray imaging. Such advanced structural studies are routinely performed at synchrotron X-ray diffraction beamlines [13]. However, applying XFEL pulses for such studies is not straightforward, as the strong excitation of valence electrons triggered by intense radiation on femtosecond timescales complicates the interpretation of the measurements. For this reason, theoretical predictions are essential to fully benefit from diffraction imaging opportunities at the XFEL facilities.

In this work, we study the effect of various hard X-ray photon energies on electronic damage and coherently scattered signals from X-ray irradiated silicon crystals. We perform computations with our hybrid code XTANT [14,15], based on the Monte Carlo (MC), Tight Binding (TB) and Molecular Dynamics (MD) simulation techniques. For realistic irradiation

Citation: Lipp, V.; Inoue I.; Ziaja, B. Advantages of Using Hard X-ray Photons for Ultrafast Diffraction Measurements. *Photonics* **2023**, *10*, 948. https://doi.org/10.3390/photonics10080948

Received: 2 June 2023
Revised: 31 July 2023
Accepted: 16 August 2023
Published: 18 August 2023

parameters, available at the SACLA XFEL facility in Japan [16], at the absorbed doses typical for serial femtosecond crystallography of inorganic materials and small-molecule systems with micrometer-size focused beams [17–19], we predict the average number of X-ray coherent and incoherent scattering events as well as the number of ionization events. The results of our simulations point out the advantage of using harder X-ray photons for ultrafast diffraction measurements.

2. Computational Approach

For the simulations, we use our in-house MC/TB/MD code XTANT [14,15]. It takes into account X-ray photon absorption by core and valence electrons, impact ionization by the photoelectrons, Auger electrons and secondary high-energy electrons (i.e., with energies above ∼10 eV). These processes are described using atomistic approximation with a classical Monte Carlo approach. The corresponding cross-sections, rates and energy levels are taken from the EPDL97 database [20], EADL97 database [21], complex dielectric function [15] and from Ref. [22]. Low-energy electrons in the valence and in the conduction band (the latter with energies below 10 eV) obey the Fermi–Dirac distribution, which is updated at every time step, taking into account how many electrons were excited to or de-excited from the high-energy electron domain. Atomic trajectories are traced with a classical MD module, using potential energy surface calculated from a TB Hamiltonian. The non-adiabatic electron–ion coupling, which leads to atomic heating on picosecond time scales, is taken into account with rate equations, including the Boltzmann collision integral [15]. The code has been successfully validated in earlier studies (for a recent review, see [15]). It provides comprehensive information about the evolution of X-ray irradiated solids, including transient electron density and temperature, electronic and atomic configuration and optical parameters.

3. Results

Using the XTANT code, we performed simulations of silicon irradiated with an X-ray pulse at photon energies of 4, 15, and 20 keV, and at X-ray absorbed doses of 1.5, 5, and 10 eV/atom [23], comparable to those used in current serial femtosecond crystallography of non-biological samples [17–19]. Here, we set the pulse duration of the X-ray pulse to 6 fs (FWHM), which is a typical value in the standard machine operation mode of SACLA [24]. For simplicity, we assumed that the sample thickness was comparable with the photon attenuation length (which is ∼10, 443 and 1038 µm for 4, 15, and 20 keV photons, respectively [25]). This results in isochoric, almost homogeneous X-ray energy absorption in the sample. Hence, we could perform constant-volume simulations for bulk silicon using a 512-atom supercell, with periodic boundary conditions.

The calculations were performed with a 5 fs time step. At each time step, the MC results were averaged over 500,000 iterations.

Figure 1 shows the evolution of the number of high- and low-energy excited electrons (the latter denoted as conduction band electrons), as well as the number of photons absorbed by time t for the case of an absorbed dose of 1.5 eV/atom. This is above the nonthermal structural damage threshold in silicon (0.9 eV/atom [23,26]). Following [26], this threshold dose can be translated into the critical number of excited conduction band electrons, which lies in this case between 0.27 and 0.4 electrons per atom. For 4 keV, 15 keV and 20 keV photon energy (Figure 1a–c), the number of excited conduction band electrons never exceeds the critical number. Note that absorbing the threshold dose yields a full disordering of the silicon structure on timescales much longer than the pulse duration of 6 fs considered here [23]. Still, some atomic dislocations may have possibly started on such a short timescale. However, at time zero, the number of excited electrons ranges from only 0.03 for 4 keV photons down to 0.006 for 20 keV photons. Because time zero corresponds to the maximal intensity of the X-ray pulse, yielding the strongest diffraction signal, such a prediction indicates that during the 6 fs long X-ray pulse, the X-ray-induced sample

damage should not significantly affect the quality of the structure determination in all the considered cases.

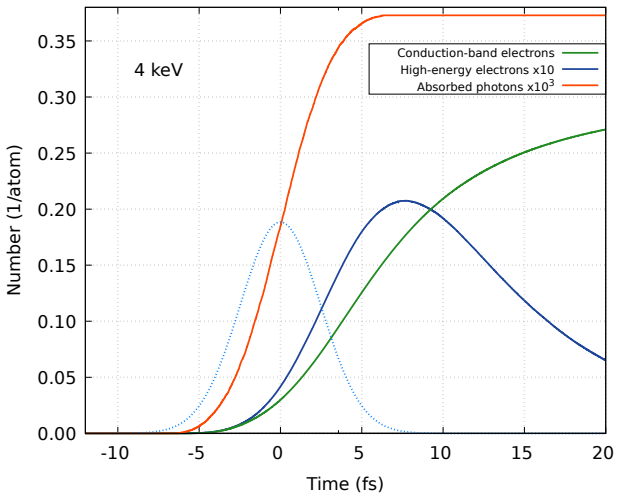

(**a**)

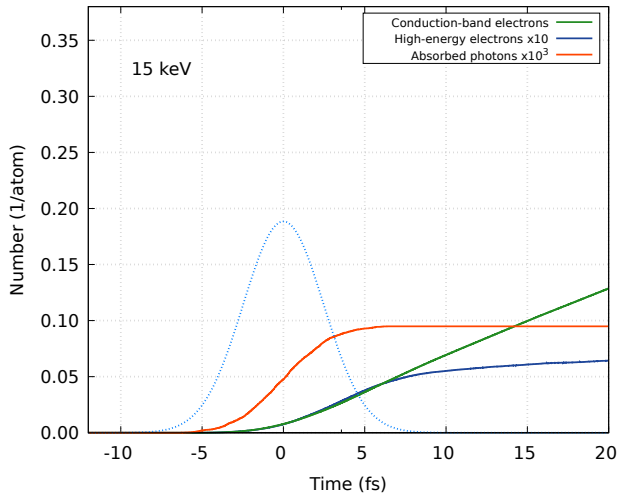

(**b**)

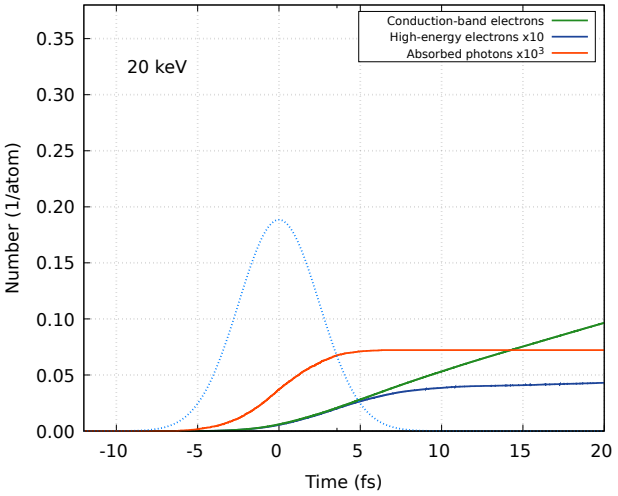

(**c**)

Figure 1. Number of conduction band (i.e., low-energy) electrons (green solid line) and high-energy electrons (blue line) in silicon as a function of time. This was calculated with the XTANT code, assuming irradiation of silicon by an X-ray pulse with 4 (**a**), 15 (**b**), and 20 keV (**c**) photons. The pulse duration was 6 fs, and the average absorbed dose was 1.5 eV/atom. The pulse shape is shown with a light-blue, dotted line in arbitrary units. The number of absorbed X-ray photons by time t is also depicted for comparison (red line).

Similar observations are made for higher absorbed doses. Figures 2 and 3 present the results regarding the number of excited electrons and absorbed photons for the X-ray absorbed doses of 5 eV/atom and 10 eV/atom, respectively. For the lowest photon energy, 4 keV, the number of excited electrons exceeds the critical electron number at the end of the pulse. However, for higher photon energies, 15 keV and 20 keV, this number never exceeds 0.20 electrons per atom. Also, at time zero, the number of excited electron per atom ranges from 0.07 for 4 keV photons down to 0.02 for 20 keV photons at the absorbed dose of 5 eV/atom, and from 0.13 for 4 keV photons down to 0.03 for 20 keV photons at the absorbed dose of 10 eV/atom. Again, like in case of the 1.5 eV/atom dose (Figure 1), the application of higher photon energies at the same absorbed dose yields a much smaller average ionization degree in the irradiated sample than in the case of the lower photon energy applied.

This shows a clear advantage of using harder X-ray photons for high-resolution crystallography. Given that the typical crystallographic reliability factor in charge density studies is in the region of a few percent [27], the small electron excitation predicted by the simulation for 20 keV photons implies the feasibility of the nearly damage-free visualization of electron density distribution even when using an intense X-ray beam providing an absorbed dose above the damage threshold.

Using the XTANT code with the electron–phonon coupling switched on (see [23]), we performed test simulations for the case of 4 keV photon energy, and 1.5 and 5 eV/atom absorbed doses. The obtained plots were indistinguishable from those obtained without the electron–phonon coupling taken into account (Figures 1a and 2a). We then concluded that the electron–ion coupling did not affect the presented results on the short time scales considered. Therefore, all the results were calculated without taking this into account, which decreased the overall computational costs.

Concerning the scattering signal, Figure 4 compares the number of coherent and incoherent photon scatterings with the number of photoabsorption events for the considered simulation conditions. The numbers were estimated with the respective cross sections taken from the NIST XCOM database [28]. This shows that the coherent scattering signal in the single-shot imaging increases with increasing photon energy, which is beneficial. The disadvantage is the increase in the incoherent signal contributing to the background. However, such an increase in the incoherent signal would not deteriorate the quality of structural studies of crystalline materials because the contribution of incoherent scattering can be readily eliminated by estimating the background signal for each Bragg spot [29].

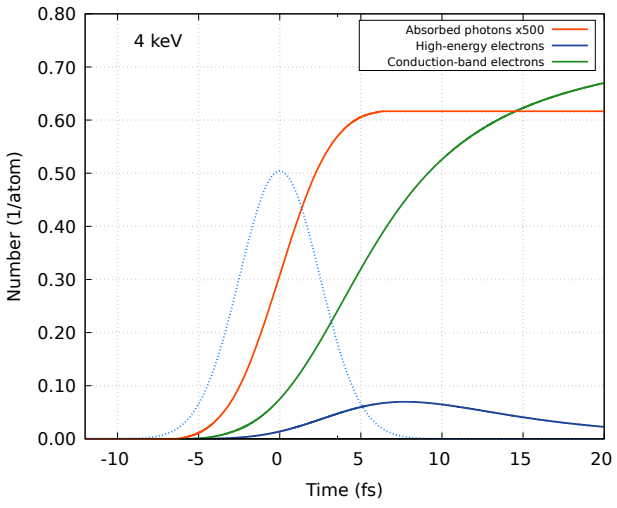

(**a**)

Figure 2. *Cont.*

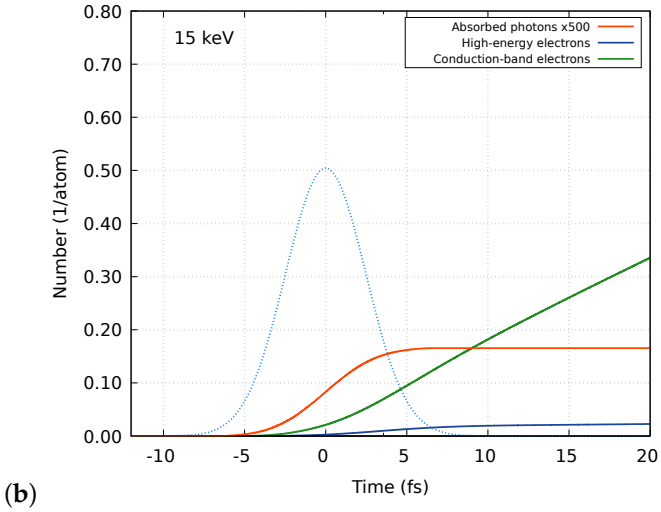

(**b**)

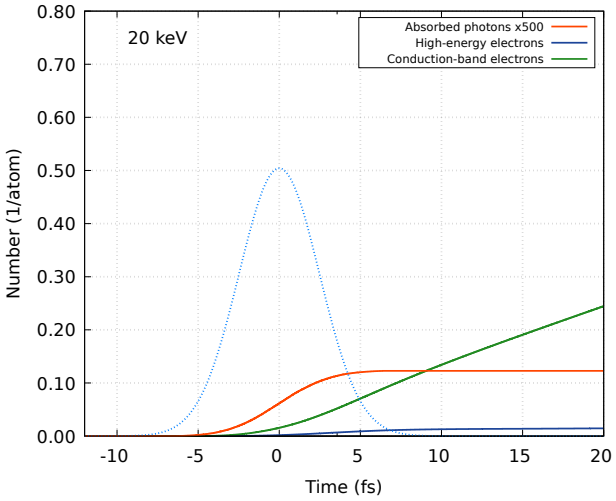

(**c**)

Figure 2. Number of conduction band (i.e., low-energy) electrons (green solid line) and high-energy electrons (blue line) in silicon as a function of time. This was calculated with the XTANT code, assuming irradiation of silicon by an X-ray pulse with 4 (**a**), 15 (**b**), and 20 keV (**c**) photons. The pulse duration was 6 fs, and the average absorbed dose was 5 eV/atom. The pulse shape is shown with a light-blue, dotted line in arbitrary units. The number of absorbed X-ray photons by time t is also depicted for comparison (red line).

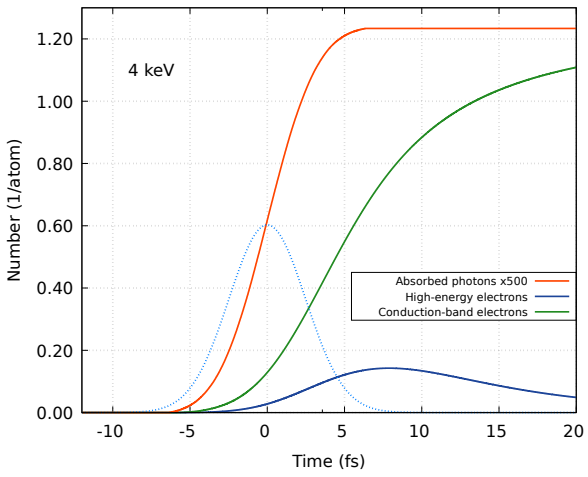

(**a**)

Figure 3. *Cont.*

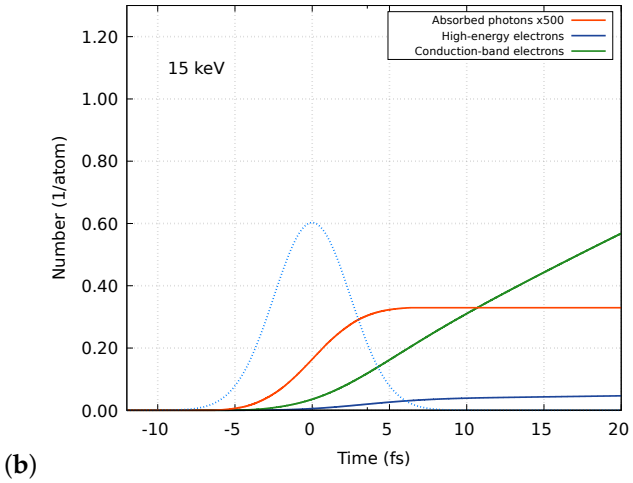

Figure 3. Number of conduction band (i.e., low-energy) electrons (green solid line) and high-energy electrons (blue line) in silicon as a function of time. This was calculated with the XTANT code, assuming irradiation of silicon by an X-ray pulse with 4 (**a**), 15 (**b**), and 20 keV (**c**) photons. The pulse duration was 6 fs, and the average absorbed dose was 10 eV/atom. The pulse shape is shown with a light-blue, dotted line in arbitrary units. The number of absorbed X-ray photons by time t is also depicted for comparison (red line).

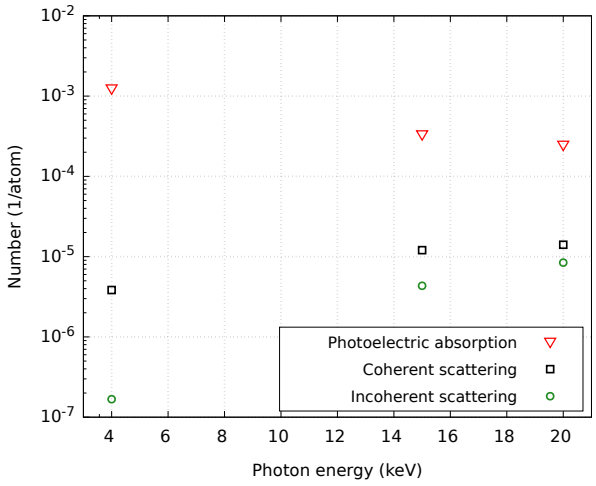

Figure 4. Number of coherent and incoherent photon scattering events and number of photoionization events in silicon during a 6 fs long FEL pulse. This was obtained for photon energies of 4, 15, and 20 keV at the absorbed dose of 5 eV/atom. The corresponding cross-sections were taken from the NIST XCOM database [28] .

4. Discussion

As we mentioned above, we assume a homogeneous energy distribution across the whole simulation volume, because we do not perform quantitative studies to be compared to the results of an experiment, but aim to identify predominant physical processes and trends, following hard X-ray irradiation. In Ref. [30], we showed how one could take the spatial pulse profile into account and perform a rigorous volume integration of the simulated diffraction signal. Such computationally expensive research is not necessary for the scope of the current work; we aim to advertise here a general idea of using hard X-rays for imaging without attempting to perform a comparison with any concrete experimental result.

Concerning the temporal pulse profile, the XFEL pulses can have a spiky structure due to the finite bandwidth (for instance, see Figure 4 of Ref. [31] and Figure 21 in Ref. [3]). When analyzing experimental data on nonlinear X-ray effects, it is important to consider these spiky structures because the instantaneous intensity can be higher than the average intensity. However, we do not expect such effects in the cases studied here, because (i) the electron photoexcitation process is linear, and (ii) the timescale of the electron photoexcitation processes is much longer than the temporal spike width. Hence, we use a temporal Gaussian pulse profile in the simulations.

Considering an eventual effect of the finite spread of pulse energy on electron excitation, since the photoabsorption cross-section will be almost the same for the whole spectral range of the XFEL pulse (which is located far from any inner-shell ionization threshold, and with very small relative energy spread of dE/E $\sim$0.3% or less), we can accurately describe the electron excitation processes using the monochromatic XFEL pulse.

Our simulations of X-ray-irradiated silicon crystals have shown that the electronic damage of the sample quantified by its average ionization degree (i.e., the number of excited conduction band electrons per atom) at a fixed absorbed dose decreases with the increasing X-ray photon energy. This also results in a much slower increase in the sample ionization degree with time for higher photon energies, increasing the onset for structural changes in the irradiated sample (see [10]). Therefore, it should be beneficial for the diffraction-before-destruction experiments to use higher-energy photons. They are already available at FEL facilities such as SACLA, for example [16].

Our study demonstrates that electronic damage can be to a large extent mitigated by the choice of proper photon energy. This opens a promising pathway towards advanced structure determination, i.e., the visualization of electron density distribution with ultrafast X-ray pulses.

5. Conclusions and Outlook

In summary, we studied electronic damage in silicon during and shortly after its irradiation with an XFEL pulse. The simulations were performed at the absorbed X-ray doses relevant for ultrafast diffraction experiments. The results demonstrate that electronic excitation becomes less significant as the photon energy increases, indicating a potential benefit of using hard X-ray photons for structure determination. In particular, the use of 20 keV XFEL pulses with a duration of 6 fs, as available at SACLA, allows the suppression of the electron excitation to the level where one can visualize electron density distribution in a nearly damage-free condition. This advantage of using hard X-ray photons also holds at higher absorbed doses, such as those typically used in diffraction experiments with silicon. Our simulations thus indicate the feasibility of charge density studies with intense XFEL pulses. This will provide new scientific opportunities that are challenging with conventional X-ray sources, such as the damage-free visualization of chemical bonding in inorganic–organic hybrid materials and the visualization of ultrafast electron transfer induced by femtosecond optical laser pulses.

Author Contributions: Conceptualization, B.Z. and I.I.; formal analysis, V.L. and B.Z.; investigation, V.L. and B.Z.; methodology, V.L. and B.Z.; software, V.L. and B.Z.; supervision, B.Z.; validation, V.L.; visualization, V.L.; writing—original draft, V.L.; writing—review and editing, V.L., B.Z. and I.I. All authors have read and agreed to the published version of the manuscript.

Funding: This research received no funding.

Data Availability Statement: The data presented in this study are available on request from the corresponding author, V.L.

Acknowledgments: We thank DESY Maxwell cluster for the computational resources.

Conflicts of Interest: The authors declare no conflict of interest.

Abbreviations

The following abbreviations are used in this manuscript:

XFEL	X-ray free-electron laser
MC	Monte Carlo
TB	Tight Binding
MD	Molecular Dynamics

References

1. Yabashi, M.; Tanaka, H. The next ten years of X-ray science. *Nat. Photonics* **2017**, *11*, 12–14. [CrossRef]
2. McNeil, B.W.; Thompson, N.R. X-ray free-electron lasers. *Nat. Photonics* **2010**, *4*, 814–821. [CrossRef]
3. Pellegrini, C.; Marinelli, A.; Reiche, S. The physics of X-ray free-electron lasers. *Rev. Mod. Phys.* **2016**, *88*, 015006. [CrossRef]
4. Neutze, R.; Wouts, R.; Van der Spoel, D.; Weckert, E.; Hajdu, J. Potential for biomolecular imaging with femtosecond X-ray pulses. *Nature* **2000**, *406*, 752–757. [CrossRef] [PubMed]
5. Gaffney, K.; Chapman, H.N. Imaging atomic structure and dynamics with ultrafast X-ray scattering. *Science* **2007**, *316*, 1444–1448. [CrossRef]
6. Boutet, S.; Lomb, L.; Williams, G.J.; Barends, T.R.; Aquila, A.; Doak, R.B.; Weierstall, U.; DePonte, D.P.; Steinbrener, J.; Shoeman, R.L.; et al. High-resolution protein structure determination by serial femtosecond crystallography. *Science* **2012**, *337*, 362–364. [CrossRef] [PubMed]
7. Chapman, H.N.; Caleman, C.; Timneanu, N. Diffraction before destruction. *Philos. Trans. R. Soc. B* **2014**, *369*, 20130313. [CrossRef]
8. Ziaja, B.; Jurek, Z.; Medvedev, N.; Saxena, V.; Son, S.K.; Santra, R. Towards Realistic Simulations of Macromolecules Irradiated under the Conditions of Coherent Diffraction Imaging with an X-ray Free-Electron Laser. *Photonics* **2015**, *2*, 256–269. [CrossRef]
9. Inoue, I.; Deguchi, Y.; Ziaja, B.; Osaka, T.; Abdullah, M.M.; Jurek, Z.; Medvedev, N.; Tkachenko, V.; Inubushi, Y.; Kasai, H.; et al. Atomic-scale visualization of ultrafast bond breaking in X-ray-excited diamond. *Phys. Rev. Lett.* **2021**, *126*, 117403. [CrossRef]
10. Inoue, I.; Tkachenko, V.; Kapcia, K.J.; Lipp, V.; Ziaja, B.; Inubushi, Y.; Hara, T.; Yabashi, M.; Nishibori, E. Delayed Onset and Directionality of X-Ray-Induced Atomic Displacements Observed on Subatomic Length Scales. *Phys. Rev. Lett.* **2022**, *128*, 223203. [CrossRef]
11. Schlichting, I. Serial femtosecond crystallography: The first five years. *IUCrJ* **2015**, *2*, 246–255. [CrossRef] [PubMed]
12. Barends, T.R.; Stauch, B.; Cherezov, V.; Schlichting, I. Serial femtosecond crystallography. *Nat. Rev. Methods Prim.* **2022**, *2*, 59. [CrossRef] [PubMed]
13. Coppens, P. *X-ray Charge Densities and Chemical Bonding*; International Union of Crystallography: Chester, UK , 1997; Volume 4.
14. Medvedev, N.; Jeschke, H.O.; Ziaja, B. Nonthermal phase transitions in semiconductors induced by a femtosecond extreme ultraviolet laser pulse. *New J. Phys.* **2013**, *15*, 015016. [CrossRef]
15. Medvedev, N.; Tkachenko, V.; Lipp, V.; Li, Z.; Ziaja, B. Various damage mechanisms in carbon and silicon materials under femtosecond X-ray irradiation. *4Open* **2018**, *1*, 3. [CrossRef]
16. Yumoto, H.; Mimura, H.; Koyama, T.; Matsuyama, S.; Tono, K.; Togashi, T.; Inubushi, Y.; Sato, T.; Tanaka, T.; Kimura, T.; et al. Focusing of X-ray free-electron laser pulses with reflective optics. *Nat. Photonics* **2013**, *7*, 43–47. [CrossRef]
17. Schriber, E.A.; Paley, D.W.; Bolotovsky, R.; Rosenberg, D.J.; Sierra, R.G.; Aquila, A.; Mendez, D.; Poitevin, F.; Blaschke, J.P.; Bhowmick, A.; et al. Chemical crystallography by serial femtosecond X-ray diffraction. *Nature* **2022**, *601*, 360–365. [CrossRef] [PubMed]
18. Støckler, L.J.; Krause, L.; Svane, B.; Tolborg, K.; Richter, B.; Takahashi, S.; Fujita, T.; Kasai, H.; Sugahara, M.; Inoue, I.; et al. Towards pump–probe single-crystal XFEL refinements for small-unit-cell systems. *IUCrJ* **2023**, *10*, 103. [CrossRef] [PubMed]
19. Takaba, K.; Maki-Yonekura, S.; Inoue, I.; Tono, K.; Hamaguchi, T.; Kawakami, K.; Naitow, H.; Ishikawa, T.; Yabashi, M.; Yonekura, K. Structural resolution of a small organic molecule by serial X-ray free-electron laser and electron crystallography. *Nat. Chem.* **2023**, *15*, 491–497. [CrossRef]
20. Cullen, D.E.; Hubbell, J.H.; Kissel, L. *EPDL97: The Evaluated Photon Data Library*; 97 Version; Technical Report; Lawrence Livermore National Lab. (LLNL): Livermore, CA, USA, 1997.

21. Perkins, S.; Cullen, D.; Chen, M.; Rathkopf, J.; Scofield, J.; Hubbell, J. *Tables and Graphs of Atomic Subshell and Relaxation Data Derived from the LLNL Evaluated Atomic Data Library (EADL). Z = 1–100*; Technical Report; Lawrence Livermore National Lab.: Livermore, CA, USA, 1991.
22. Palik, E.D. *Handbook of Optical Constants of Solids*; Academic Press: San Diego, CA, USA, 1985.
23. Medvedev, N.; Li, Z.; Ziaja, B. Thermal and nonthermal melting of silicon under femtosecond x-ray irradiation. *Phys. Rev. B* **2015**, *91*, 054113. [CrossRef]
24. Inoue, I.; Hara, T.; Inubushi, Y.; Tono, K.; Inagaki, T.; Katayama, T.; Amemiya, Y.; Tanaka, H.; Yabashi, M. X-ray Hanbury Brown-Twiss interferometry for determination of ultrashort electron-bunch duration. *Phys. Rev. Accel. Beams* **2018**, *21*, 080704. [CrossRef]
25. Henke, B.; Gullikson, E.; Davis, J. X-ray interactions: Photoabsorption, scattering, transmission, and reflection at E = 50–30.000 eV, Z = 1–92. *At. Data Nucl. Data Tables* **1993**, *54*, 181–342. [CrossRef]
26. Follath, R.; Koyama, T.; Lipp, V.; Medvedev, N.; Tono, K.; Ohashi, H.; Patthey, L.; Yabashi, M.; Ziaja, B. X-ray induced damage of B_4C-coated bilayer materials under various irradiation conditions. *Sci. Rep.* **2019**, *9*, 2029. [CrossRef]
27. Koritsanszky, T.S.; Coppens, P. Chemical applications of X-ray charge-density analysis. *Chem. Rev.* **2001**, *101*, 1583–1628. [CrossRef]
28. Berger, M.J.; Hubbell, J.H.; Seltzer, S.M.; Chang, J.; Coursey, J.S.; Sukumar, R.; Zucker, D.S.; Olsen, K. XCOM: Photon Cross Sections Database. **2010**, NIST, PML, Radiation Physics Division. https://dx.doi.org/10.18434/T48G6X (accessed on 17 August 2023).
29. White, T.A.; Kirian, R.A.; Martin, A.V.; Aquila, A.; Nass, K.; Barty, A.; Chapman, H.N. CrystFEL: A software suite for snapshot serial crystallography. *J. Appl. Crystallogr.* **2012**, *45*, 335–341. [CrossRef]
30. Tkachenko, V.; Abdullah, M.M.; Jurek, Z.; Medvedev, N.; Lipp, V.; Makita, M.; Ziaja, B. Limitations of Structural Insight into Ultrafast Melting of Solid Materials with X-ray Diffraction Imaging. *Appl. Sci.* **2021**, *11*, 5157. . [CrossRef]
31. Inubushi, Y.; Tono, K.; Togashi, T.; Sato, T.; Hatsui, T.; Kameshima, T.; Togawa, K.; Hara, T.; Tanaka, T.; Tanaka, H.; et al. Determination of the Pulse Duration of an X-Ray Free Electron Laser Using Highly Resolved Single-Shot Spectra. *Phys. Rev. Lett.* **2012**, *109*, 144801. [CrossRef] [PubMed]